Enhanced Charge Transfer Kinetics for the Electroreduction of Carbon Dioxide on Silver Electrodes Functionalized with Cationic Surfactants

Wei Jie Teh[a], *Manuel J. Kolb*[b], *Federico Calle-Vallejo*[b,c,d,*], *Boon Siang Yeo*[a,*]

[a] Department of Chemistry, National University of Singapore, 3 Science Drive 3, Singapore 117543.

[b] Department of Materials Science and Chemical Physics & Institute of Theoretical and Computational Chemistry (IQTCUB), University of Barcelona, Martí i Franquès 1, 08028 Barcelona, Spain.

[c] Nano-Bio Spectroscopy Group and European Theoretical Spectroscopy Facility (ETSF), Department of Polymers and Advanced Materials: Physics, Chemistry and Technology, University of the Basque Country UPV/EHU, Avenida Tolosa 72, 20018 San Sebastián, Spain.

[d] IKERBASQUE, Basque Foundation for Science, Plaza de Euskadi 5, 48009 Bilbao, Spain.

* To whom correspondence should be addressed: BSY (Email: chmyeos@nus.edu.sg) or FCV (Email: federico.calle@ehu.es).

Keywords: electrochemical CO_2 reduction, surfactants, silver, electrocatalysis, electrochemical impedance spectroscopy, density functional theory, carbon monoxide

Abstract

Cationic ammonium surfactants can be used together with a suitable catalyst to enhance the electroreduction of carbon dioxide (CO_2RR). However, the underlying reasons for the improvements are not yet well understood. In this work, it is shown that didodecyldimethylammonium bromide (DDAB; $[(C_{12}H_{25})_2N(CH_3)_2]Br$), when added to the catholyte, can increase the rate of CO_2 reduction to CO on silver electrodes by 12-fold at −0.9 V versus reversible hydrogen electrode. More importantly, electrochemical impedance spectroscopy revealed that DDAB lowered the charge transfer resistance (R_{CT}) for CO_2RR on silver, and these changes can be correlated with enhancements in partial current densities of CO. Interestingly, when DDAB is added onto two other CO-producing metals, namely, zinc and gold, the CO_2RR charge transfer kinetics are improved only on Zn, but not on Au electrodes. By means of a semiempirical model combining density functional theory calculations and experimental data, it is concluded that DDAB generally strengthens the adsorption energies of the *COOH intermediate, which leads to enhanced CO production on silver and zinc, but not on gold.

1. Introduction

The electrocatalytic reduction of carbon dioxide (CO_2RR) using renewable energies is a promising method to produce chemicals and fuels.[1–3] Among the many possible reaction products, carbon monoxide (CO) is highly desirable as it is used as a feedstock in industrial processes such as the Fischer-Tropsch synthesis.[1,4,5] Ag, Au, and Zn electrodes are known to favor the selective reduction of CO_2 to CO.[6–9] However, hurdles such as the sluggish kinetics of the CO_2RR and the competing hydrogen evolution reaction (HER) still need to be overcome, in order for the electrochemical conversion of CO_2 to CO to become an industrially-viable process.[10–12]

CO production can be enhanced by nanostructuring the electrode surface[13–18] and by increasing the solubility of CO_2 in the electrolyte.[19,20] More recently, the addition of cationic ammonium surfactants into the electrolyte has helped improve the rate of CO_2RR, mainly by suppressing the parasitic HER.[21–26] Banerjee et al. reported an increase in partial current densities for CO (j_{CO}) on Cu from ~ −0.05 to −0.4 mA cm^{-2} at −0.77 V vs. RHE (all potentials stated hereafter are referenced to the RHE) after cetyltrimethylammonium bromide (CTAB, $[(C_{16}H_{33})N(CH_3)_3]Br$) was added, and showed that CTAB decreased HER during CO_2RR.[27] They hypothesized that the suppression of HER was due to H^+ species being displaced at the electrode double layer by cationic surfactants containing long hydrophobic tails. Quan et al. reported a 98 % Faradaic efficiency (FE) for CO and a 1.5-fold rise in j_{CO} to −4.0 mA cm^{-2} on Ag electrodes at −0.9 V when dodecyltrimethylammonium bromide (DTAB, $[(C_{12}H_{25})N(CH_3)_3]Br$) was used as a surfactant.[28] These authors also proposed that the surfactants mainly suppressed the HER. Recently, Buckley et al. reported a FE_{CO} of 97 % and a nine-fold increase in j_{CO} from −0.14 to −1.21 mA cm^{-2} at −0.8 V on Ag electrodes, with complete suppression of the HER when dihexadecyldimethylammonium bromide (DHDAB, $[(C_{16}H_{33})_2N(CH_3)_2]Br$) was added.[29] Ge et al. similarly observed a FE_{CO} of 96 % and an

increase in j_{CO} from −2.5 to −4.1 mA cm^{-2} at −0.9 V on Ag electrodes when CTAB was added in 0.5 M $KHCO_3$.[30] Both groups hypothesized that the improved CO_2 reduction was caused by the added surfactants increasing the local CO_2 concentrations and hydrophobicity near the electrode surface. Interestingly, we found no works attributing the increase in j_{CO} when surfactants are added to the electrolyte to enhanced CO_2RR charge transfer kinetics or improvements in the binding energies of *COOH, which is a key intermediate of CO_2RR to CO.[14,31]

In this work, we investigate whether surfactants could enhance CO_2RR by improving the CO_2RR charge transfer kinetics. Previous studies have shown that coating didodecyldimethylammonium bromide (DDAB, $[(C_{12}H_{25})_2N(CH_3)_2]Br$) on carbon electrodes can boost the electron transfer rate between the Fe^{2+}/Fe^{3+} redox couple in proteins by up to a thousand times.[32,33] In this respect, DDAB is an appealing cationic surfactant for amplifying the kinetics of CO_2 reduction to CO. Indeed, we discover that adding DDAB to the catholyte significantly boosts the charge transfer kinetics for CO_2RR to CO on silver catalysts, while slowing the HER charge transfer kinetics. In the presence of DDAB, j_{CO} increased by 12-fold to −5.5 mA cm^{-2} at −0.9 V. Using electrochemical impedance spectroscopy, we show that changes in CO_2RR are correlated to changes in its R_{CT}. We further built a semiempirical model using density functional theory (DFT) and experimental data to illustrate how DDAB functionalization strengthens the adsorption energy of *COOH during CO_2RR to CO. This is the first work detailing how cationic surfactants improve the charge transfer kinetics of CO_2RR, which in turn enhances j_{CO}. Finally, using the guidelines of our model and combining the effects of surface roughness and surfactant functionalization, we engineered anodized Ag electrodes with DDAB for CO_2RR, resulting in a j_{CO} of –10.6 mA cm^{-2} at –0.9 V.

2. Results and discussion

2.1. Electrocatalytic CO_2RR on Ag electrodes with DDAB

Electrochemical measurements were performed in a H-cell containing a Ag/AgCl (saturated KCl) reference electrode and a graphite rod counter electrode (Supporting Information, Section S1). Mechanically polished Ag discs (geometric surface area = 0.385 cm^2) were employed as working electrodes. The electrolyte was CO_2-saturated 0.1 M $KHCO_3$ (pH ~6.8). During experiments, CO_2 was continually bubbled into the cathodic chamber at a flow rate of 10 sccm. For measurements using surfactant-functionalized electrodes, we added different amounts of DDAB (6.6, 66, 330 and 660 μM) to the catholyte (**Table S1)**. Overall, we found that 66 μM of DDAB in CO_2-saturated 0.1 M $KHCO_3$ (pH ~6.8) is optimal for CO_2RR. Hence, this will be the concentration of DDAB used for the experiments described hereafter.

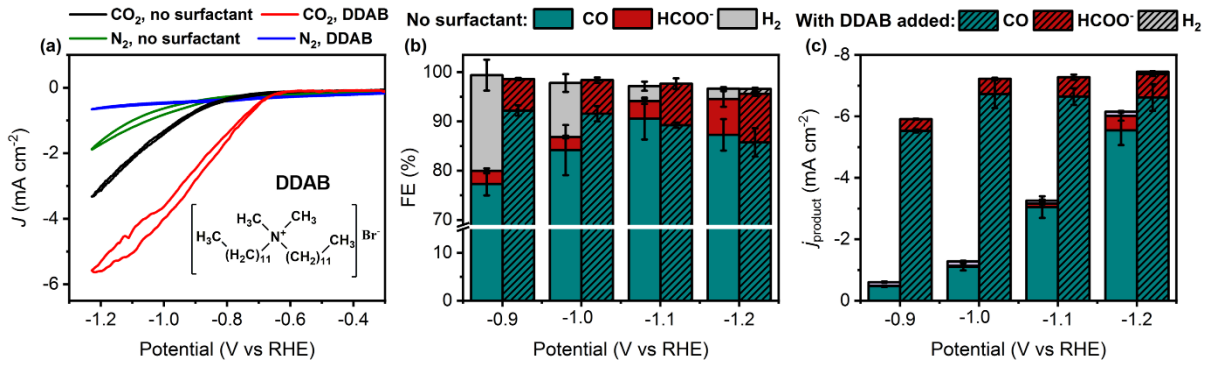

Figure 1. (a) Cyclic voltammograms of a silver electrode in 0.1 M $KHCO_3$ and 0.1 M $KHCO_3$ + 66 μM DDAB electrolytes under CO_2- or N_2-saturation. The chemical structure of DDAB is shown in the inset. (b) Faradaic efficiencies and (c) current densities of products formed from a silver electrode during chronoamperometry at different potentials. The electrolyte used was 0.1 M $KHCO_3$ and 0.1 M $KHCO_3$ + 66 μM DDAB under CO_2-saturation. Duration of chronoamperometry: 40 min.

The effects of DDAB on CO_2RR were first studied using cyclic voltammetry (**Figure 1a)**. Under CO_2-saturation, the total current densities improved when DDAB was added. For example, at −1.0 V, the total current density increased from −1.4 to −4 mA cm^{-2} (unless specified, all current densities reported here and after are normalized to the geometric surface area of the electrode). Interestingly, under N_2-saturation conditions, the current densities were lower in the presence of DDAB.

The activity and selectivity of CO_2RR in the presence of DDAB was further quantified at fixed potentials from −0.9 to −1.2 V (**Figures 1b-c**). CO, formate ($HCOO^-$) and H_2 were the only products detected, and their FEs add up to 97-98 %. At −0.9 V, after DDAB was added, the FE_{CO} rose from 77 to 92 %; j_{CO} was boosted 12 times from −0.47 to −5.5 mA cm^{-2}. j_{CO} then plateaued at ~ −6.7 mA cm^{-2} from −1.0 to −1.2 V with DDAB added. In contrast, without DDAB in the electrolyte, j_{CO} increased continuously from −0.47 mA cm^{-2} at −0.9 V to −5.5 mA cm^{-2} at −1.2 V. The addition of DDAB also resulted in the formation of more $HCOO^-$. For instance, the partial current densities of $HCOO^-$ (j_{HCOO-}) rose from −0.02 to −0.38 mA cm^{-2} at −0.9 V after DDAB was added. It is noteworthy that when DDAB was added, no H_2 was detected during CO_2RR from −0.9 to −1.1 V (**Figure S2**); H_2 was only detected at −1.2 V. We also measured the Tafel slopes of CO_2RR to CO in electrolytes with and without DDAB (**Figure S3**). Without DDAB, the Tafel slope was 126 mV dec^{-1}, which is consistent with values reported in previous works.[14,34] When DDAB was added, the Tafel slope decreased from 126 to 92 mV dec^{-1}, indicating that adding DDAB increases the rate of CO_2RR to CO on Ag. Altogether, these observations indicate that DDAB enhances CO_2RR on Ag, while inhibiting HER.

To ascertain if the plateauing of j_{CO} in **Figure 1c** is due to CO_2 mass-transport limitations, we conducted CO_2RR with a higher CO_2 flow rate at −1.0 V with DDAB added (**Table S4**). When the CO_2 flow rate was increased from 10 to 30 sccm, j_{CO} increased from −6.7 to −10.6 mA cm^{-2}. This indicates that the plateau in j_{CO} is indeed likely due to CO_2 mass-transport limitations. The enhancement in j_{CO} under a higher CO_2 flow rate can be attributed to a thinner CO_2 boundary layer at the electrode surface, which in turn increased the flux and local concentration of CO_2 at the electrode.[35–37]

We then assessed if the increase in j_{CO} with DDAB added can be sustained over time (**Figure S4**). CO production at −1.0 V was maintained for 10 h (FE_{CO} and j_{CO} varied

respectively between 90 to 94 % and −6.2 to −6.9 mA cm^{-2}). No changes in the concentrations of DDAB were observed before and after the stability tests, which attests to its structural durability (**Table S5**).

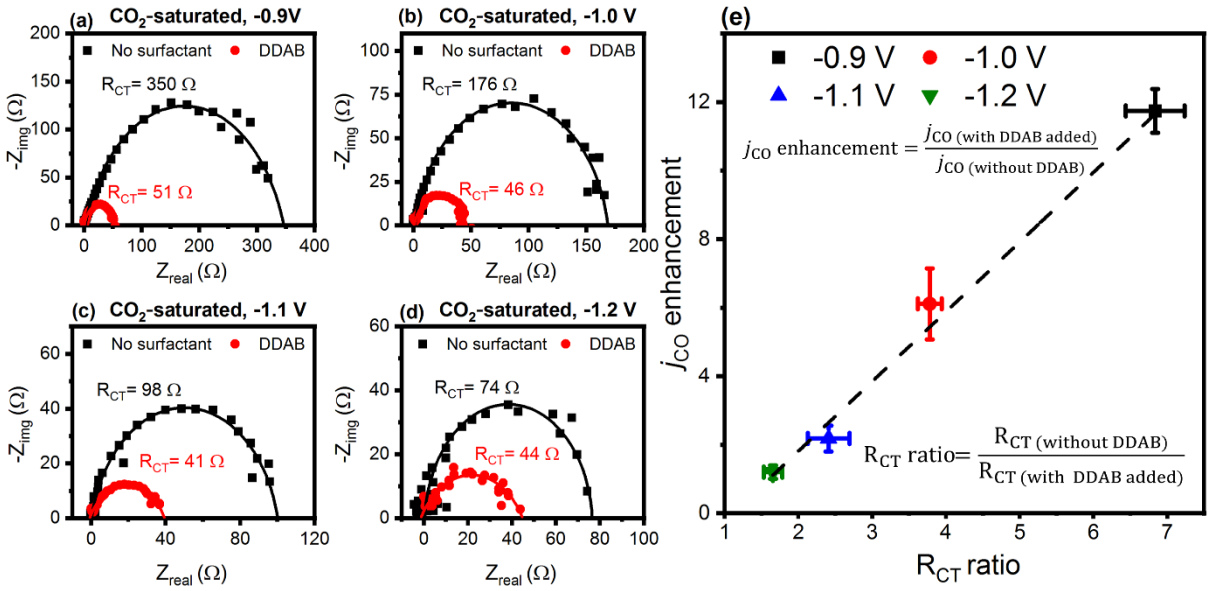

Figure 2. (a-d) Nyquist plots for Ag discs in CO_2-saturated 0.1 M $KHCO_3$ and 0.1 M $KHCO_3$ + 66 μM DDAB electrolytes at −0.9, −1.0, −1.1 and −1.2 V. For clarity, the solution resistance was removed from each plot. (e) Enhancement in j_{CO} at different applied potentials with respect to the R_{CT} ratio, after DDAB was added. The dashed line is drawn to guide the eye. A larger R_{CT} ratio will lead to a more significant enhancement in j_{CO} during CO_2RR.

2.2. Analyzing CO_2RR charge transfer kinetics using EIS

We used electrochemical impedance spectroscopy (EIS) to study how DDAB affects charge transfer kinetics during CO_2RR. The R_{CT} values were measured from −0.9 to −1.2 V under CO_2-saturation (**Figures 2a-d, Section S2.5**), where CO_2RR is the main charge transfer process. At −0.9 V, the R_{CT} with DDAB added was 51 Ω, which was ~7 times lower than the R_{CT} without DDAB (350 Ω). At −1.0, −1.1 and −1.2 V, the R_{CT} values, in the presence of DDAB, were ~3.8, 2.4 and 1.7 times lower than the R_{CT} values without DDAB, respectively. The enhancement in j_{CO} at different potentials when DDAB was added to the electrolyte could be correlated with a decrease in R_{CT} values (**Figure 2e**). We also note that the R_{CT} value at −0.9 V with DDAB added (51 ± 2 Ω) is smaller than the R_{CT} value at −1.2 V without DDAB

(74 ± 3 Ω). This indicates that adding DDAB to Ag is a more important factor in improving the CO_2RR charge transfer kinetics, compared to applying a more negative potential **(Figure S5)**.

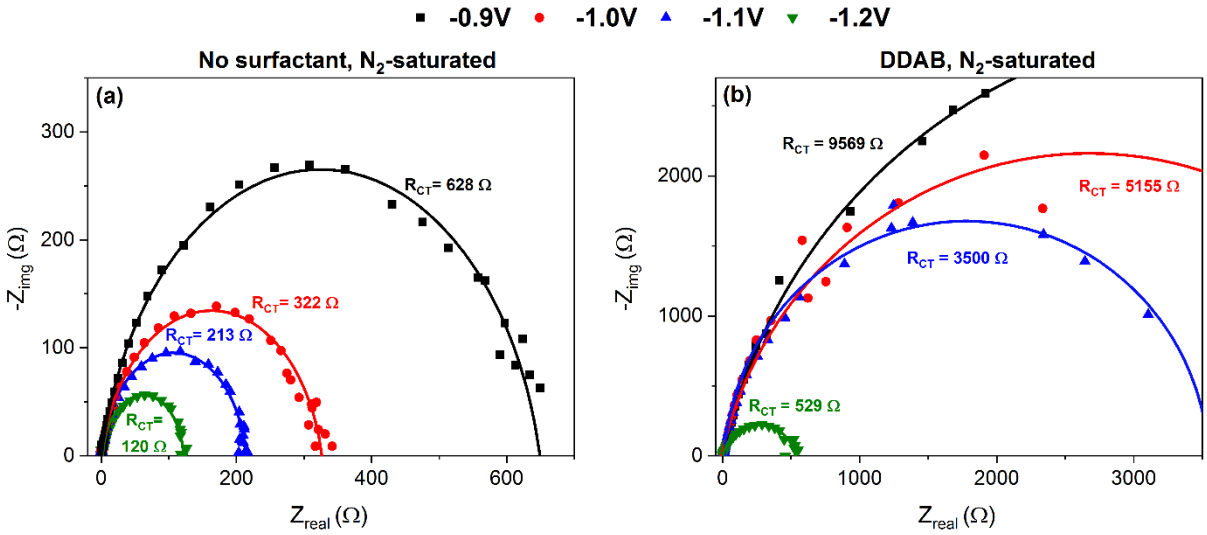

Figure 3. Nyquist plots for Ag disc electrodes measured at various potentials in N_2-saturated (a) 0.1 M $KHCO_3$ and (b) 0.1 M $KHCO_3$ + 66 μM DDAB electrolytes, respectively. For clarity, the solution resistance was removed from each plot.

We further conducted EIS experiments on Ag electrodes in N_2-saturated 0.1 M $KHCO_3$ electrolytes, where HER is the sole charge-transfer process (**Figure 3**). Interestingly, R_{CT} increased when DDAB was added to the electrolyte. This contrasts with the decrease in R_{CT} observed when DDAB was added under CO_2-saturated conditions. The large R_{CT} values of 3500 to 9569 Ω measured at −0.9 to −1.1 V with DDAB added also coincided with no HER being observed during CO_2RR (Figures 1b-c). At −1.2 V, the R_{CT} decreased to 529 Ω, which is also the potential in which H_2 first evolved during CO_2RR with DDAB added (Figures 1b-c). Overall, the above findings show that DDAB induces two effects: it enhances charge-transfer processes for CO_2RR and suppresses HER.

We have considered if the aforementioned improvements in CO_2RR to CO were due to increases in CO_2 solubilities in electrolytes containing DDAB (**Table S6**). The CO_2 concentration in CO_2-saturated 0.1 M $KHCO_3$ with DDAB added was thus measured (1230 ± 73 ppm = 28 ± 2 mM), but was found similar to that without DDAB

(1250 ± 31 ppm = 29 ± 1 mM). This indicates that CO_2 solubility is not enhanced by the addition of DDAB to the electrolyte. We also investigated whether surface roughening of the electrode by DDAB might be a cause for the rise in j_{CO}. Towards this end, scanning electron microscopy (SEM) was performed on the Ag electrodes before and after they were used for CO_2RR in the presence of DDAB (**Figure S6**). No notable changes in the electrode surface were observed after CO_2RR. This is further corroborated by double layer capacitance (C_{dl}) measurements on the Ag electrodes (C_{dl} values are directly proportional to the electrochemically active surface areas (ECSA), see **Figure S7**).[38,39] After CO_2RR in the presence of DDAB, the Ag electrode was washed with water to remove DDAB from the surface. The C_{dl} of the rinsed Ag electrode (0.047 mF cm^{-2}) was similar to the C_{dl} of a freshly polished Ag electrode (0.047 mF cm^{-2}). This indicates that adding DDAB to the electrolyte does not change the ECSA of Ag. The ECSA-normalized j_{CO} at −1.0 V for Ag with DDAB added (−6.7 mA cm^{-2}) was also ~6.5 times higher than that observed without DDAB (−1.1 mA cm^{-2}, **Table S7**). This further suggests that the addition of DDAB does improve the intrinsic activity of CO production on Ag.

We then determined if varying the anion, carbon chain length and number of C_{12} carbon chain branches in the ammonium cationic surfactants will affect CO_2RR charge-transfer kinetics on Ag (**Figure 4, Section S2.8**). CO_2RR was performed at −1.0 V using didodecyldimethylammonium chloride (DDAC, $[(C_{12}H_{25})_2N(CH_3)_2]Cl$, different anion), didecyldimethylammonium bromide (DAB, $[(C_{10}H_{21})_2N(CH_3)_2]Br$, shorter carbon chain length), DHDAB ($[(C_{16}H_{33})_2N(CH_3)_2]Br$, longer carbon chain length), DTAB ($[(C_{12}H_{25})N(CH_3)_3]Cl$, one C_{12} branch) or tridodecylmethylammonium chloride (TDAC, $[(C_{12}H_{25})_3N(CH_3)]Cl$, three C_{12} branches). In the presence of these surfactants, j_{CO} increases with decreasing R_{CT} (**Figure 4b**). The results from the addition of DDAC indicate that changing the halide counter ion from Br^- to Cl^- has no significant effect on the CO_2RR activity. However,

we highlight that having a halide anion (either Br^- or Cl^-) is still crucial for surfactant-mediated CO_2RR, which will be explained later by means of DFT calculations. Under N_2-saturation, the addition of DDAC, TDAC, and DHDAB resulted in an increased R_{CT} of 4298, 1840, and 3625 Ω, respectively, and this is correlated with the total suppression of the HER (Section S2.8, **Figure S8**). In brief, we conclude that the greatest enhancement in CO_2RR activity on Ag was found using an ammonium salt surfactant with either Br^- or Cl^- and two chains of C_{12}. Surfactants with one or three C_{12} branches are not as favorable for CO production. Surfactants with carbon chains that are longer or shorter than 12 carbons are also deleterious for CO production.

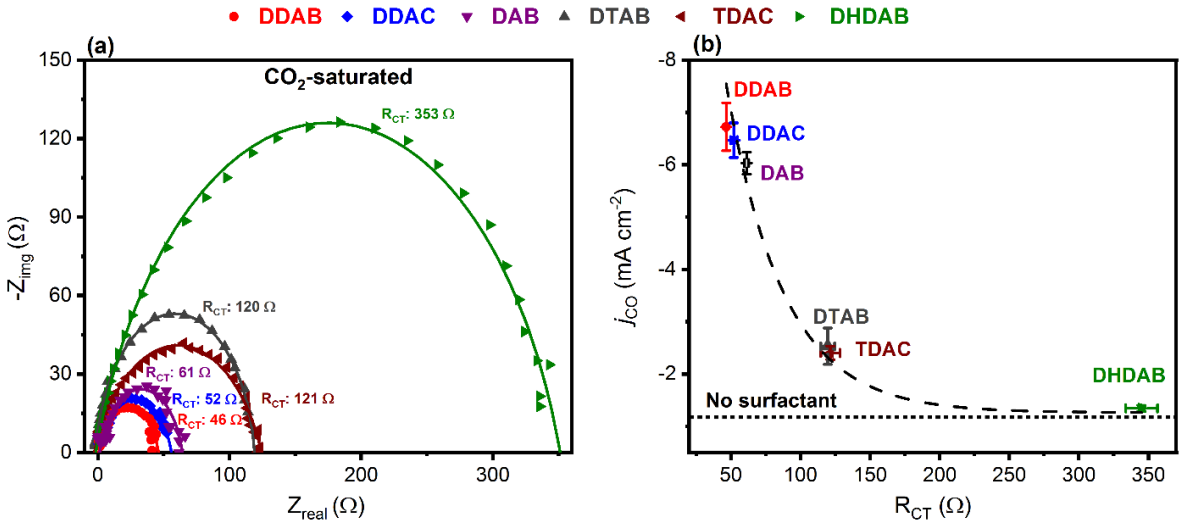

Figure 4. (a) Nyquist plots for Ag disc electrodes in CO_2-saturated 0.1 M $KHCO_3$ electrolyte + 66 μM of various surfactants, namely DDAB, DDAC, DAB, DHDAB, DTAB or TDAC. The applied potential was −1.0 V. For clarity, the solution resistance was removed from each plot. (b) Dependence of j_{CO} on R_{CT} in the presence of various surfactants on Ag electrodes (the dashed curve is added to guide the eye; the horizontal dashed line indicates the j_{CO} measured in the absence of a surfactant).

2.3. CO_2RR performance on Zn and Au electrodes with DDAB

We now examine the effects of DDAB on the CO_2RR performance of Zn and Au, which are also CO-producing metals.[6] CO_2RR was conducted at −1.0 V. When DDAB was added to Zn during CO_2RR, j_{CO} increased from −0.5 to −5.7 mA cm^{-2} (**Figure 5a**), while the R_{CT} values decreased from 200 Ω to 74 Ω (**Figure 5b**). Under N_2-saturation, the partial current densities of H_2 (j_{H2}) diminished from −0.37 to −0.09 mA cm^{-2}, which can be correlated to an increase in

R_{CT} from 195 to 339 Ω (**Figure 5c**). These changes in j_{CO} and j_{H2} are comparable to those found on Ag electrodes. Interestingly, both j_{CO} and j_{H2} decreased when DDAB was added to Au during CO_2RR (Figure 5a). This corresponded to an increase in R_{CT} from 113 Ω to 237 Ω under CO_2-saturated conditions (**Figure 5d**) and from 111 Ω to 218 Ω under N_2-saturated conditions (**Figure 5e**).

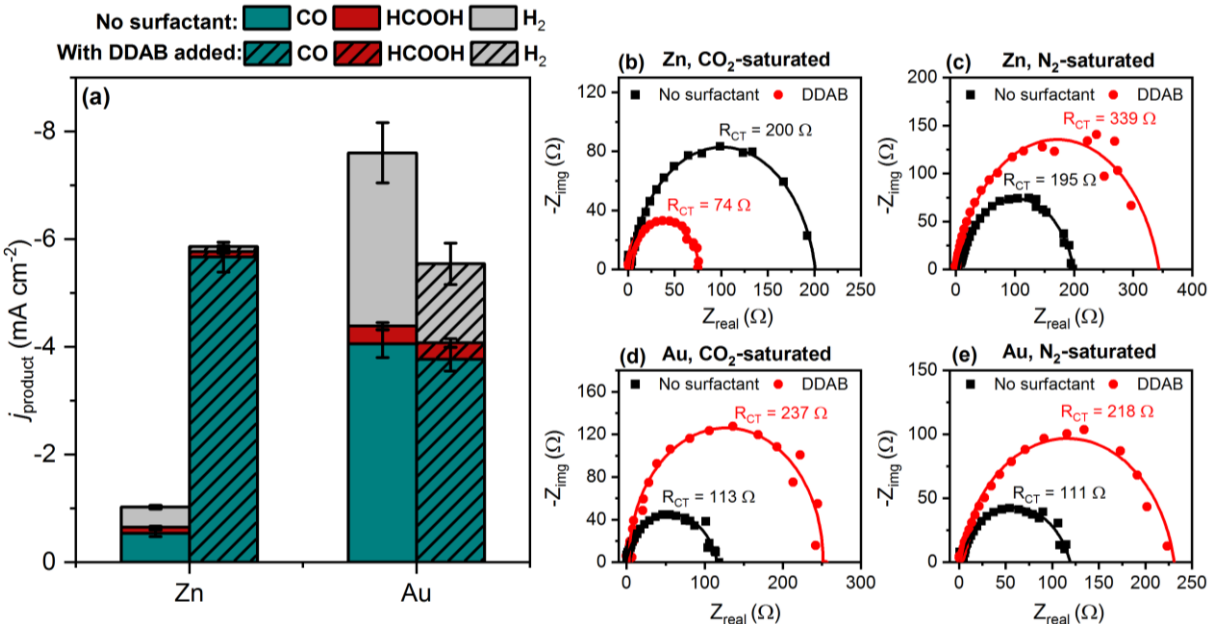

Figure 5. (a) Current densities of products formed during CO_2 electrolysis on zinc and gold electrodes in 0.1 M $KHCO_3$ and 0.1 M $KHCO_3$ + 66 μM DDAB electrolyte at −1.0 V. Nyquist plots of (b-c) Zn, and (d-e) Au discs in 0.1 M $KHCO_3$ and 0.1 M $KHCO_3$ + 66 μM DDAB under CO_2- or N_2-saturated conditions. The potential applied was −1.0 V. For clarity, the solution resistance was removed from each plot.

We investigated whether the changes in j_{CO} on the Zn or Au electrodes were due to surface roughening by DDAB. No changes in the ECSAs were observed after electrolysis (**Figure S9**). We then assessed if the decrease in j_{CO} on the Au electrode was due to the absence of DDAB on its surface. To study this, the C_{dl} values of Ag, Au, and Zn electrodes in electrolytes without DDAB, and with 6.6 to 660 μM of DDAB added were measured. The C_{dl} was measured using EIS at −1.0 V and under CO_2-saturation (**Figure S10**). With 66 μM of DDAB, the C_{dl} reduced from 0.037 to 0.018 mF cm^{-2} on Ag electrodes, from 0.039 to 0.033 mF cm^{-2} on Zn electrodes, and from 0.058 to 0.011 mF cm^{-2} on Au electrodes. The C_{dl} then plateaued on all surfaces, with 66 to 660 μM of DDAB added. This decrease in C_{dl} can be

attributed to an increase in hydrophobicity at the electrode surface in the presence of DDAB.[22,27] This indicates that DDAB is indeed present on all three electrode surfaces during electrolysis. We note that the change in C_{dl} only accounts for the presence of DDAB on the electrode but does not indicate its exact coverage.

2.4. Semiempirical modelling of surfactant effects on CO_2RR to CO and $HCOO^-$

We now combine experimental and DFT-calculated results in a simple semiempirical model to analyze how surfactants impact the CO_2RR activities of Ag, Au, and Zn electrodes. To avoid computational pitfalls related to decoupled proton-electron transfers, the reduction of CO_2 to CO ($CO_{2(g)} + 2H^+ + 2e^- \rightarrow CO_{(g)} + H_2O_{(l)}$) is usually assumed to proceed through the elementary steps in Equations 1-3:[14,40,41]

$$^* + CO_{2(g)} + H^+ + e^- \rightarrow {}^*COOH \quad (1)$$

$$^*COOH + H^+ + e^- \rightarrow {}^*CO + H_2O_{(l)} \quad (2)$$

$$^*CO \rightarrow {}^* + CO_{(g)} \quad (3)$$

The lone asterisk (*) denotes a free surface site and an asterisk next to a chemical species indicates that the species is adsorbed. Similarly, the reduction of CO_2 to $HCOO^-$ ($CO_{2(g)} + H^+ + 2e^- \rightarrow HCOO^-_{(l)}$) is assumed to proceed as:

$$^* + CO_{2(g)} + H^+ + e^- \rightarrow {}^*OCHO \quad (4)$$

$$^*OCHO + e^- \rightarrow {}^* + HCOO^- \quad (5)$$

Various works have highlighted that the adsorption energies of *COOH and *CO (ΔG_{COOH} and ΔG_{CO}) are suitable descriptors for the trends in CO production on metal electrodes, while the adsorption energy of *OCHO (ΔG_{OCHO}) captures the trends in $HCOO^-$ production.[10,31,42] Here, the adsorption energies of those three adsorbates on Ag, Au and Zn

electrodes in the presence and absence of a simplified version of DDAB (and DDAC for Ag) with shorter organic tails were calculated (**Figures S16-S18**). We found that the surfactant generally strengthens the adsorption energies of the adsorbates on the three metals.

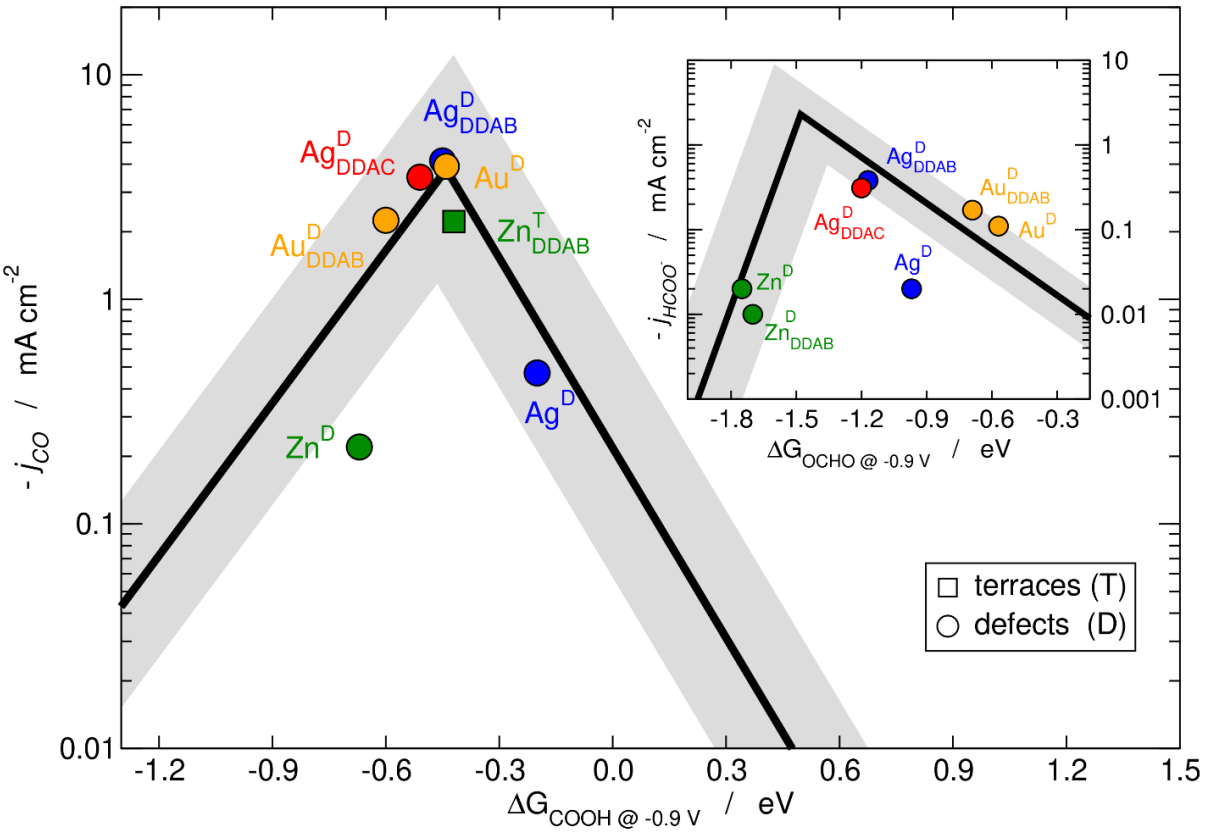

Figure 6. Trends in the partial current densities of Ag, Au, and Zn at −0.9 V for CO_2 reduction to CO (main panel) and $HCOO^-$ (inset) as a function of the adsorption energies of *COOH and *OCHO at −0.9 V before and after the addition of DDAB and DDAC. T: terrace sites (squares), D: defect sites (circles). The grey band spans over ±0.2 eV around the abscissae of the black lines and corresponds to the accuracy of DFT. Only the most active sites are shown in this figure. An extended version of it with all sites is presented in Figure S19, together with the raw data and the equations of the lines (Section S3).

To rationalize the effects, we will consider that the experimental current densities on all substrates were contributed by the closest-packed surfaces ((111) terraces for Ag and Au, (0001) terraces for Zn) and defects (step edges at Ag(211), Au(110), and Zn(105), see **Section S3** and previous works[9,41,43] for justifications on these choices). For each substrate, the total current density is: $j_i^{total} = j_i^T + j_i^D$, where T and D stand for terraces and defects, and i = CO and $HCOO^-$. The partial current densities of CO per site at −0.9 V are plotted in **Figure 6** as a function of the adsorption energies of *COOH, with the volcano lines obtained by linear

regression of literature data[31,42] (see further details in Section S3). The intersection of the lines, which indicates the peak of j_{CO}, lies at a *COOH adsorption energy of −0.44 eV.

For clarity, only the adsorption energies of the most active sites are shown in Figure 6 (an extended version with all data is presented in **Figure S19** and all data are shown in **Table S17**). We observe that defects are the most active sites on Ag and Au with (Ag^{D}_{DDAB} and Au^{D}_{DDAB}) and without (Ag^{D} and Au^{D}) surfactant added, whereas the most active sites on Zn are the defects when there is no surfactant and the terraces upon addition of DDAB. Initially, *COOH adsorbed on Ag^{D} is located on the weak-binding side of the plot. In the presence of the surfactant, the -OH moiety of *COOH interacts with the anionic part of the surfactant, while the =O moiety interacts with the cationic tail of the surfactant (Figure S16). These adsorbate-surfactant interactions strengthen the binding of *COOH on Ag, pushing it to the top of the volcano and resulting in an optimized j_{CO}. This indicates that using a surfactant with too few C_{12} chains or short carbon chains may result in insufficient adsorbate-surfactant interactions, while having too many C_{12} chains or long carbon chains in the surfactant result in steric hindrance and loss of anionic interactions. This conclusion agrees with the optimal surfactant configuration of two C_{12} chains, as shown in Figure 4, and highlights the need for both cationic and anionic interactions, as shown in **Figure S12**.

Conversely, Au^{D} is initially located at the peak, and that the strengthening of *COOH by adding DDAB leads to poorer CO production. It is noteworthy that the deactivation of Au defects is partially counteracted by the simultaneous activation of its terrace sites upon addition of DDAB (Figure S19). Finally, Zn defects are on the strong-binding side of the volcano and Zn terraces are on the weak-binding side (Figures 6 and S19). Because surfactant-adsorbate interactions stabilize the adsorption energies of *COOH, DDAB significantly enhances Zn terraces for CO production while Zn defects remain far from the top of the volcano.

In the case of $HCOO^-$ production, Ag, Au, and Zn sites are all far from the peak of the volcano (located at $\Delta G_{OCHO} \approx -1.48\, eV$, see the inset of Figure 6). While the addition of DDAB visibly enhances the production of $HCOO^-$ on Ag, the changes in *OCHO adsorption energies and current densities on Au and Zn are scant. According to Figure S17, only one of the O atoms in *OCHO interacts with the cationic part of the surfactant, which explains why the enhancement of ΔG_{OCHO} is smaller than that of ΔG_{COOH} when DDAB is added (Table S17). We note that Zn^D lies slightly out of the grey band in Figure 6, while Ag^D falls outside the grey band in the inset. The former deviation is rationalized based on previous work, which found that the most active Zn sites for CO_2RR to CO are less coordinated than step-edge sites[9] and bind *COOH more strongly. The latter deviation is explained by considering that Ag defects are the most active sites for both CO and $HCOO^-$ production but tend to be CO-selective.

We also modelled the adsorption energies of the *H intermediate on Ag terraces and defects to determine how adding DDAB affects H_2 evolution **(Figure S20)**. Because Ag is a weak-binding catalyst, Ag defects are more HER-active by virtue of their stronger binding energies compared to Ag terraces. The presence of DDAB, however, weakens the binding energies of *H on the Ag defects. This indicates that adding DDAB to the electrolyte will result in HER suppression during CO_2 electrolysis. However, we emphasize that Ag itself is already a poor HER catalyst,[44] as evidenced by the low partial current densities of H_2 in Figure 1c.

We further found that changing the surfactant from DDAB to DDAC resulted in differences in adsorption energies of only ~0.05 eV for both *COOH and *OCHO on Ag (Figure 6, Table S17). This corroborates with the similar j_{CO} and j_{HCOO-} observed with both DDAB- and DDAC-modified Ag catalysts. We also evaluated the effects of anions alone on the catalyst surface by calculating the adsorption energies of *COOH and *OCHO on Ag in the presence of *Br and *Cl. The halides alone destabilize both *COOH and *OCHO instead of

stabilizing them (**Figures** S12 and **S13**), indicating that the improvement in CO_2RR activity with surfactants is not merely an anion effect but also induced by the cationic chains.

In brief, our calculations indicate that surfactants generally strengthen the adsorption energies of adsorbed intermediates of CO_2RR to CO and $HCOO^-$. Semiempirical modelling shows that the active sites for CO production upon addition of DDAB are the Ag defects, both terraces and defects on Au, and terraces on Zn. In turn, the active sites for $HCOO^-$ production upon adding DDAB are the defects for Ag, Au, and Zn. However, all three metals are far from the top of the volcano for $HCOO^-$ production and are CO-selective, making it difficult for adsorption-site engineering to increase $HCOO^-$ production.

The main guideline for catalyst design which we extract from Figure 6 is to first increase the number of defects on Ag electrodes, followed by the addition of DDAB. This should result in a maximized CO production, while $HCOO^-$ production would only be modestly improved. To verify this prediction, CO_2RR was conducted at −0.9 V on anodized Ag electrodes (highly defective surface) in the presence of DDAB (**Table S12, Figure S11**). Indeed, a twofold enhancement in j_{CO} was observed on anodized Ag (−10.6 mA cm^{-2}) as compared to polished Ag (−5.5 mA cm^{-2}) . This experimental result on anodized Ag also validates our semiempirical assessment that Ag defects are the key active sites for CO production when DDAB is added: according to our model, the maximum j_{CO} on Ag terraces with DDAB is −1.36 mA cm^{-2} (Table S17), implying that the j_{CO} from Ag defects on anodized Ag with DDAB is about −9.24 mA cm^{-2}, which is ~87 % of the overall j_{CO} of −10.6 mA cm^{-2} measured on anodized Ag. In the case of $HCOO^-$ production, j_{HCOO-} on anodized Ag with DDAB was found to be −0.45 mA cm^{-2}, similar to that on polished Ag (−0.38 mA cm^{-2}). These observations validate our assessment on CO_2RR catalyst design, and our design guideline is therefore promising for the design of advanced nanostructured electrodes.

3. Conclusions

In this work, we employed the surfactant DDAB to boost the reduction of CO_2 to CO on Ag electrodes. The addition of DDAB induces a 12-fold enhancement of j_{CO} from −0.47 to −5.5 mA cm^{-2} and completely suppressed H_2 evolution at −0.9 V. EIS measurements showed that adding DDAB lowered R_{CT} for the CO_2RR and increased it for the HER on Ag electrodes. These findings indicate that DDAB primarily enhanced CO_2RR charge-transfer processes, while suppressing HER charge transfer on Ag. The addition of DDAB also boosts CO_2RR charge-transfer kinetics on Zn electrodes, but not on Au electrodes. We propose that cationic ammonium surfactants improve CO_2RR to CO via the stabilization of the key CO_2RR intermediate, i.e., *COOH. There is also a strengthening of the *OCHO adsorption energies, but it is insufficient to result in large amounts of $HCOO^-$ being produced during CO_2RR, as Ag, Au and Zn all lie far from the top of the volcano-shaped activity plot.

Experimental section

Detailed experimental procedures and characterization methods can be found in Section S1, Supporting information. Theoretical procedures, gas-phase and liquid-phase corrections, specific free energy values including ZPE and TS corrections, and the coordinates of the optimized slabs can be found in Sections S3 and S4, Supporting information.

Supporting Information

Supporting Information is available from the Wiley Online Library or from the author.

Acknowledgements

The authors thank the National University of Singapore (A-0004135-00-00) and National Research Foundation of Singapore (Urban Solutions and Sustainability, Industry Alignment Fund (Pre-Positioning) Programme, A-0004543-00-00) for financial support of this project. The grants RTI2018-095460-B-I00, RYC-2015-18996, and MDM-2017-0767 were funded by MCIN/AEI/ 10.13039/501100011033 and by the European Union. The use of supercomputing facilities at SURFsara was sponsored by NWO Physical Sciences, with financial support by NWO.

Received: ((will be filled in by the editorial staff))
Revised: ((will be filled in by the editorial staff))
Published online: ((will be filled in by the editorial staff))

References

[1] O. S. Bushuyev, P. De Luna, C. T. Dinh, L. Tao, G. Saur, J. van de Lagemaat, S. O. Kelley, E. H. Sargent, *Joule* **2018**, *2*, 825.

[2] Y. Y. Birdja, E. Pérez-Gallent, M. C. Figueiredo, A. J. Göttle, F. Calle-Vallejo, M. T. M. Koper, *Nat. Energy* **2019**, *4*, 732.

[3] S. Nitopi, E. Bertheussen, S. B. Scott, X. Liu, A. K. Engstfeld, S. Horch, B. Seger, I. E. L. Stephens, K. Chan, C. Hahn, J. K. Nørskov, T. F. Jaramillo, I. Chorkendorff, *Chem. Rev.* **2019**, *119*, 7610.

[4] M. E. Dry, *J. Chem. Technol. Biotechnol.* **2002**, *77*, 43.

[5] S. Hernández, M. A. Farkhondehfal, F. Sastre, M. Makkee, G. Saracco, N. Russo, *Green Chem.* **2017**, *19*, 2326.

[6] Y. Hori, H. Wakebe, T. Tsukamoto, O. Koga, *Electrochim. Acta* **1994**, *39*, 1833.

[7] T. Hatsukade, K. P. Kuhl, E. R. Cave, D. N. Abram, T. F. Jaramillo, *Phys. Chem. Chem. Phys.* **2014**, *16*, 13814.

[8] E. R. Cave, J. H. Montoya, K. P. Kuhl, D. N. Abram, T. Hatsukade, C. Shi, C. Hahn, J.

K. Nørskov, T. F. Jaramillo, *Phys. Chem. Chem. Phys.* **2017**, *19*, 15856.

[9] M. P. L. Kang, M. J. Kolb, F. Calle-Vallejo, B. S. Yeo, *Adv. Funct. Mater.* **2022**, 2111597.

[10] A. Bagger, W. Ju, A. S. Varela, P. Strasser, J. Rossmeisl, *ChemPhysChem* **2017**, *18*, 3266.

[11] P. De Luna, C. Hahn, D. Higgins, S. A. Jaffer, T. F. Jaramillo, E. H. Sargent, *Science* **2019**, *364*, eaav3506.

[12] E. O. Eren, S. Özkar, *J. Power Sources* **2021**, *506*, 230215.

[13] W. Luo, J. Zhang, M. Li, A. Züttel, *ACS Catal.* **2019**, *9*, 3783.

[14] J. Rosen, G. S. Hutchings, Q. Lu, S. Rivera, Y. Zhou, D. G. Vlachos, F. Jiao, *ACS Catal.* **2015**, *5*, 4293.

[15] S. Mezzavilla, S. Horch, I. E. L. Stephens, B. Seger, I. Chorkendorff, *Angew. Chem., Int. Ed.* **2019**, *58*, 3774.

[16] A. S. Hall, Y. Yoon, A. Wuttig, Y. Surendranath, *J. Am. Chem. Soc.* **2015**, *137*, 14834.

[17] Y. Chen, C. W. Li, M. W. Kanan, *J. Am. Chem. Soc.* **2012**, *134*, 19969.

[18] L. Q. Zhou, C. Ling, M. Jones, H. Jia, *Chem. Commun.* **2015**, *51*, 17704.

[19] S. Lamaison, D. Wakerley, J. Blanchard, D. Montero, G. Rousse, D. Mercier, P. Marcus, D. Taverna, D. Giaume, V. Mougel, M. Fontecave, *Joule* **2020**, *4*, 395.

[20] R. M. Arán-Ais, D. Gao, B. Roldan Cuenya, *Acc. Chem. Res.* **2018**, *51*, 2906.

[21] Y. Zhong, Y. Xu, J. Ma, C. Wang, S. Sheng, C. Cheng, M. Li, L. Han, L. Zhou, Z. Cai, Y. Kuang, Z. Liang, X. Sun, *Angew. Chem., Int. Ed.* **2020**, *59*, 19095.

[22] O. Gutiérrez-Sánchez, N. Daems, M. Bulut, D. Pant, T. Breugelmans, *ACS Appl. Mater. Interfaces* **2021**, *13*, 56205.

[23] L. Chen, F. Li, Y. Zhang, C. L. Bentley, M. Horne, A. M. Bond, J. Zhang, *ChemSusChem* **2017**, *10*, 4109.

[24] Z. Tao, Z. Wu, Y. Wu, H. Wang, *ACS Catal.* **2020**, *10*, 9271.

[25] Z. Q. Zhang, S. Banerjee, V. S. Thoi, A. Shoji Hall, *J. Phys. Chem. Lett.* **2020**, *11*, 5457.

[26] S. Banerjee, Z. Q. Zhang, A. S. Hall, V. S. Thoi, *ACS Catal.* **2020**, *10*, 9907.

[27] S. Banerjee, X. Han, V. S. Thoi, *ACS Catal.* **2019**, *9*, 5631.

[28] F. Quan, M. Xiong, F. Jia, L. Zhang, *Appl. Surf. Sci.* **2017**, *399*, 48.

[29] A. K. Buckley, T. Cheng, M. H. Oh, G. M. Su, J. Garrison, S. W. Utan, C. Zhu, F. D. Toste, W. A. Goddard, F. M. Toma, *ACS Catal.* **2021**, *11*, 9034.

[30] W. Ge, Y. Chen, Y. Fan, Y. Zhu, H. Liu, L. Song, Z. Liu, C. Lian, H. Jiang, C. Li, *J. Am. Chem. Soc.* **2022**, *144*, 6613.

[31] J. T. Feaster, C. Shi, E. R. Cave, T. Hatsukade, D. N. Abram, K. P. Kuhl, C. Hahn, J. K. Nørskov, T. F. Jaramillo, *ACS Catal.* **2017**, *7*, 4822.

[32] M. Li, J. Wang, B. Sun, N. Li, Z. Gu, *J. Electrochem. Soc.* **2004**, *151*, E271.

[33] J. F. Rusting, A. E. F. Nassar, *J. Am. Chem. Soc.* **1993**, *115*, 11891.

[34] Y. C. Hsieh, L. E. Betancourt, S. D. Senanayake, E. Hu, Y. Zhang, W. Xu, D. E. Polyansky, *ACS Appl. Energy Mater.* **2019**, *2*, 102.

[35] N. Gupta, M. Gattrell, B. MacDougall, *J. Appl. Electrochem.* **2006**, *36*, 161.

[36] J. C. Bui, C. Kim, A. Z. Weber, A. T. Bell, *ACS Energy Lett.* **2021**, *6*, 1181.

[37] E. L. Clark, J. Resasco, A. Landers, J. Lin, L. T. Chung, A. Walton, C. Hahn, T. F. Jaramillo, A. T. Bell, *ACS Catal.* **2018**, *8*, 6560.

[38] E. L. Clark, S. Ringe, M. Tang, A. Walton, C. Hahn, T. F. Jaramillo, K. Chan, A. T. Bell, *ACS Catal.* **2019**, *9*, 4006.

[39] S. Trasatti, O. A. Petrii, *Pure Appl. Chem.* **1991**, *63*, 711.

[40] H. A. Hansen, J. B. Varley, A. A. Peterson, J. K. Nørskov, *J. Phys. Chem. Lett.* **2013**, *4*, 388.

[41] L. P. Granda-Marulanda, A. Rendón-Calle, S. Builes, F. Illas, M. T. M. Koper, F. Calle-Vallejo, *ACS Catal.* **2020**, *10*, 6900.

[42] K. P. Kuhl, T. Hatsukade, E. R. Cave, D. N. Abram, J. Kibsgaard, T. F. Jaramillo, *J. Am. Chem. Soc.* **2014**, *136*, 14107.

[43] A. Rendón-Calle, S. Builes, F. Calle-Vallejo, *Appl. Catal. B* **2020**, *276*, 119147.

[44] E. R. Cave, C. Shi, K. P. Kuhl, T. Hatsukade, D. N. Abram, C. Hahn, K. Chan, T. F. Jaramillo, *ACS Catal.* **2018**, *8*, 3035.

Adding didodecyldimethylammonium bromide (DDAB) to silver electrodes during CO_2 electroreduction (CO_2RR) significantly enhances the rate of CO production. Electrochemical impedance spectroscopy shows that adding DDAB improves the CO_2RR charge transfer kinetics. A semiempirical model further shows that the improvements in CO production and charge transfer kinetics are due to DDAB strengthening the binding energies of the *COOH intermediate during CO_2RR.

Wei Jie Teh, Manuel J. Kolb, Federico Calle-Vallejo*, Boon Siang Yeo*

Enhanced Charge Transfer Kinetics for the Electroreduction of Carbon Dioxide on Silver Electrodes Functionalized with Cationic Surfactants